Blade-Loss-Caused Rubbing Dynamic Characteristics of Rotor-Bladed Disk-Casing System

Zeng Jin[1], *Ma Hui*[1,2*], *Ma Xinxing*[1], *Wu Zhiyuan*[3], *Qin Zhaoye*[4]

1. School of Mechanical Engineering and Automation, Northeastern University, Shenyang 110819, P. R. China;
2. State Key Laboratory of Mechanical System and Vibration, Shanghai Jiao Tong University, Shanghai 200240, P. R. China; 3. Shanghai Institute of Space Power-Sources, Shanghai 200245, P. R. China;
4. Department of Mechanical Engineering, Tsinghua University, Beijing 100084, P. R. China

(Received 9 December 2017; revised 14 January 2018; accepted 20 January 2018)

Abstract: Considering the elastic supports, the finite element model of rotor-bladed disk-casing system is established using commercial software ANSYS/LS-DYNA. Assuming that broken blade is released from the disk, the complicate rubbing responses of unbalanced rotor-bladed disk-casing system are studied under different operational speeds. In addition, influences of both plastic deformation of blade and casing failure are analyzed. The results show that there exist some multiple even fractional frequencies in the transient and steady vibration responses of unbalanced rotor. Besides, one nodal diameter vibration of bladed disk coupling with the lateral vibration of the shaft as well as the first order bending vibration of blade can be excited under low operational speed, while the first order bending vibration of blade coupling with the lateral vibration of disk-shaft is easily excited under high operational speed. During rubbing process, three distinct contact states can be observed: broken blade-casing contact, broken blade-blade component-casing contact and broken blade-casing contact/blade component-casing contact/blade self-contact. It is worth noting that the third contact state is related to the operational speed. With the increase of operational speed, self-contact in the blade may occur.

Key words: rotor-bladed disk-casing system; blade loss; rubbing; casing failure; elastic supports

CLC number: TP391.9 **Document code**: A **Article ID**: 1005-1120(2018)01-0116-10

0 Introduction

Aero-engine usually operates in harsh working conditions such as high temperature, high pressure and high speed[1-2]. Accordingly, rotor, bladed disk, casing and bearing, as the key components of aero-engine, often suffer from the combined alternating effects of centrifugal, aerodynamic and thermal loads[3-4]. Therefore, fatigue crack is easily initiated under these circumstances. According to the existing literatures, blade crack is studied by many scholars as a common problem[5-8]. Once the crack generates, then propagates rapidly and fractures finally[9]. Released rotating blade can further perforate the casing as well as other airplane components and endangers the flight safety[10-11]. Therefore, blade containment test must be conducted during engine development[9]. However, due to high experimental cost and less useful datum, numerical simulation is mostly adopted to carry out blade containment analysis in many cases[10-12]. Sun et al.[13] simplified the dual-rotor as a lumped mass model, and casing is established by mixed beam-solid elements. Besides, the coupling effects between rotors and casing are considered through spring elements. Then dynamics of the system due to blade loss event is discussed. Con-

* Corresponding author, E-mail address: mahui_2007@163.com.

How to cite this article: Zeng Jin, Ma Hui, Ma Xinxing, et al. Blade-loss-caused rubbing dynamic characteristics of rotor-bladed disk-casing system[J]. Trans. Nanjing Univ. Aero. Astro., 2018,35(1):116-125.
http://dx.doi.org/10.16356/j.1005-1120.2018.01.116

sidering the effects of blade loss. Sinha[14] derived the equations of motion of unsymmetrical rotor-bladed disk system using analytical methods, and discussed the rubbing characteristics between blade and rigid casing. Based on LS-DYNA software, Carney et al.[12] and Jain et al.[15] simulated the interaction process between blade fragment, rotor and casing as well as the motion trajectory of local components. Heidari et al.[16] adopted implicit-explicit-implicit analysis process to discuss the complicated rubbing dynamics of whole aero-engine based on MD Nastran software. He et al.[17-19] combined numerical simulation with experiments to carry out the research on blade containment, and the results obtained from LS-DYNA agreed well with those obtained from experiments.

According to the literatures listed above, blade containment and blade loss-induced rubbing dynamics between unbalanced rotor and casing are the two main topics concerned by many scholars. As for the research on blade containment, rotor and bearing supports are usually removed from the system. As for blade loss-induced rubbing dynamics between unbalanced rotor and casing, most researchers simulate blade loss effect only through introducing unbalanced force but ignoring blade loss-induced asymmetrical inertia and mass variation of the system, moreover, material property of the components is often linear elastic and casing flexibility is paid less attention. Therefore, this paper mainly combines the blade containment with blade loss-induced rubbing dynamics, and establishes a single rotor-bladed disk-casing system using commercial software ANSYS/LS-DYNA. Then the complicated rubbing characteristics between blade fragment, casing and unbalanced rotor system are simulated. In addition, vibration responses of disk mass center, changing rules of rubbing force and contact states among system components are also analyzed in detail. Finally, some conclusions are made.

1 Finite Element Model of Rotor-Bladed Disk-Casing System

The finite element model of rotor-bladed disk-casing system is shown in Fig. 1. In Fig. 1, rotor, bladed disk and casing are meshed by solid element Solid164, and bearing supports are simulated by spring/damping element Combin165. Furthermore, gap between blade tip and casing is defined as 0.8 mm. Table 1 lists the material parameters of corresponding components. After finite element discretization, the equations of motion of the system can be written as follows

$$\boldsymbol{M}\ddot{\boldsymbol{u}} + (\boldsymbol{C} + \boldsymbol{G}(\omega))\dot{\boldsymbol{u}} + (\boldsymbol{K} + \boldsymbol{K}(\omega))\boldsymbol{u} = \boldsymbol{R} + \boldsymbol{R}_c \quad (1)$$

where $\boldsymbol{M}$, $\boldsymbol{C}$ and $\boldsymbol{K}$ are the mass matrix, damping matrix and structural stiffness matrix of the system; $\boldsymbol{G}(\omega)$ and $\boldsymbol{K}(\omega)$ the gyroscopic and stiffness matrices corresponding to operational speed ω ($\omega = \pi n/30$, n represents the operational speed and its unit is 'rev/min'), respectively; $\boldsymbol{R}$ and $\boldsymbol{R}_c$ the external load and contact force, respectively; $\ddot{\boldsymbol{u}}$, $\dot{\boldsymbol{u}}$ and $\boldsymbol{u}$ the acceleration, velocity and displacement of the system, respectively.

In this paper, blade loss is released from the disk and simulated by elements deletion (see Fig. 1(b)). Because of solid elements lacking rotational freedoms, in order to make the rotor-bladed disk system rotate about the z-axis (see Fig. 1(a)), the regions being 5 mm away from left and right shaft ends are defined as rigid bodies (see Fig. 1(d)), and only u_x, u_y and rot z are unconstrained. Considering that casing is a kind of thin-shell structure and may be destroyed by rotating broken blade, the failure stress of casing is defined as 902 MPa. Moreover, since the contact between components cannot be predicted in advance, the eroding-single-surface contact type is adopted in the system, and this can be helpful to simulate complicated contact behaviors between components.

Fig. 2 shows the local modes of rotor-bladed disk - casing system . Figs. 2 (a, b) represent the

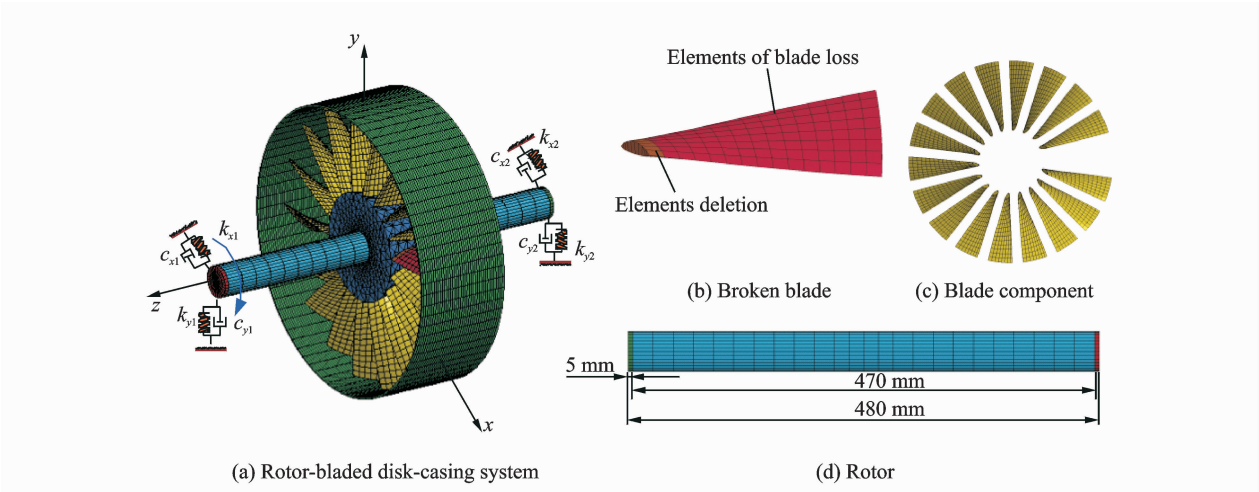

Fig. 1 Finite element model of rotor-bladed disk-casing system

Table 1 Parameter settings for rotor-disk-blades system with spring-damping supports

Component	Density ρ/(kg·m^{-3})	Young's modulus E/MPa	Poisson's ratio υ	Tangent modulus G/MPa	Yield strength σ_s/ MPa	Stiffness k_{xi}, k_{yi}/(N·m^{-1}) (i=1,2)	Damping c_{xi}, c_{yi}/(N·s·m^{-1}) (i=1,2)
Rotor	7 850	2.066×10^5	0.3				
Disk	7 850	2.066×10^5	0.3				
Blade	4 370	1.25×10^5	0.3	927	825		
Casing	4 370	1.25×10^5	0.3	927	825		
Spring-damper						$k_{x1}=2.7\times10^8$ $k_{y1}=4.89\times10^8$ $k_{x2}=9.4\times10^7$ $k_{y2}=7.67\times10^8$	$c_{x1}=3.84\times10^5$ $c_{y1}=6.08\times10^5$ $c_{x2}=1.33\times10^5$ $c_{y2}=1.89\times10^6$

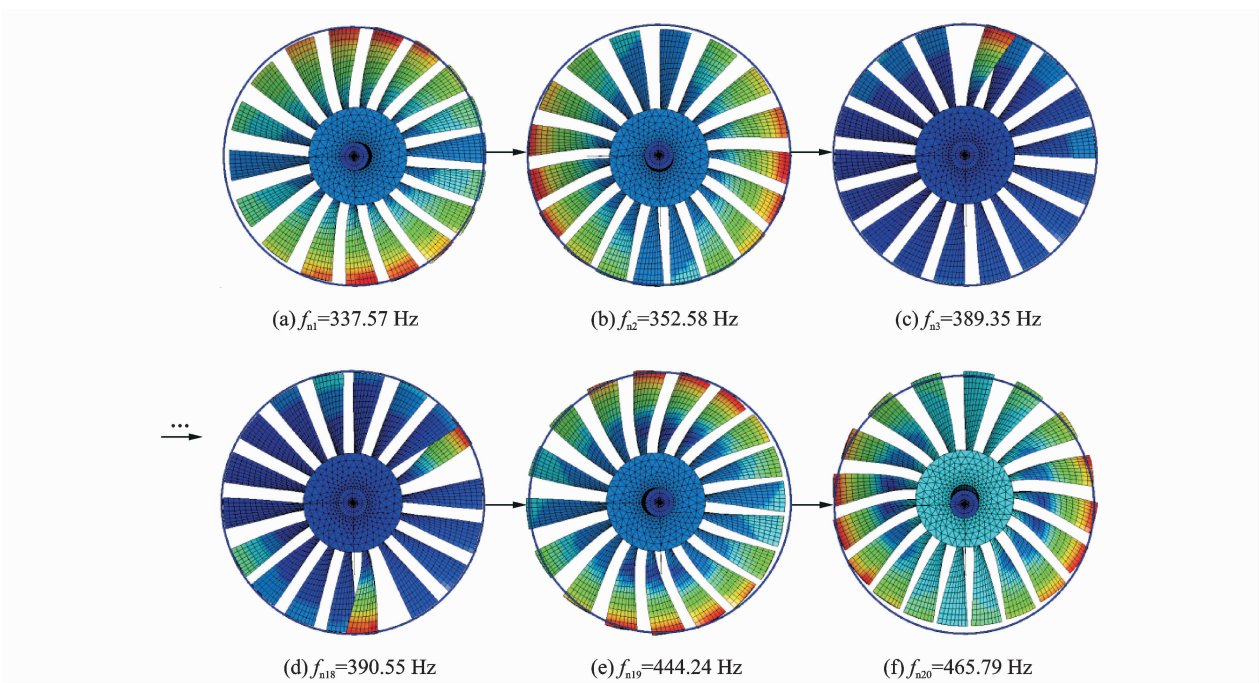

Fig. 2 Local modes of rotor-bladed disk-casing system

the one nodal diameter vibration of bladed disk coupling with the lateral vibration of shaft. Figs. 2 (c, d) show the first order bending vibration of blade. Figs. 2 (e, f) show the first order bending vibration of blade coupling with the lateral vibration of disk-shaft.

Rayleigh damping is adopted in the system when conducting transient dynamic analysis. Corresponding formula is written as follows

$$\begin{cases} \boldsymbol{C}=\alpha\boldsymbol{M}+\beta\boldsymbol{K} \\ \alpha=2(\xi_2/\omega_2-\xi_1/\omega_1)/(1/\omega_2^2-1/\omega_1^2) \\ \beta=(2\xi_2\omega_2-\xi_1\omega_1)/(\omega_2^2-\omega_1^2) \end{cases} \quad (2)$$

where $\omega_1=2\pi f_1$, $\omega_2=2\pi f_2$, $\xi_1=\xi_2=0.02$. [f_1, f_2] and ξ_1, ξ_2 are the concerned low-frequency range covering the first 20 order natural frequencies (see Fig. 2) and damping ratios. In this paper, f_1 and f_2 equal 300 Hz and 500 Hz, respectively.

In order to consider the effect of initial stress caused by the operational speed on the vibration response of the system, an implicit-explicit sequence solution is adopted, and corresponding flow chart is shown in Fig. 3.

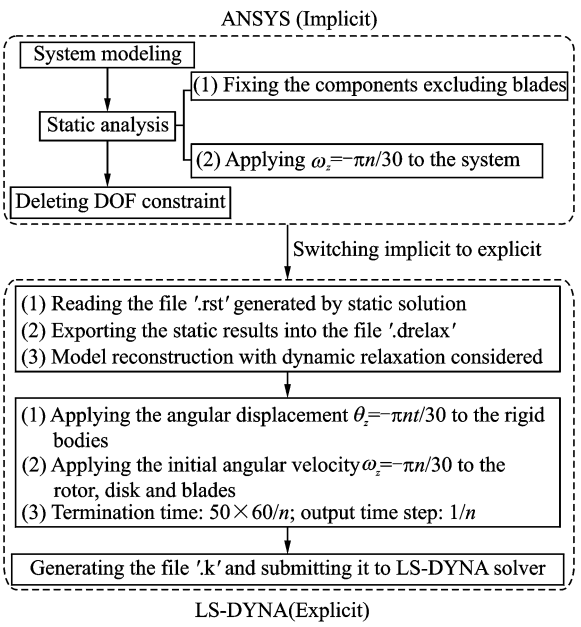

Fig. 3 Implicit-explicit analysis flow chart of the rotor-bladed disk-casing system

2 Dynamic Characteristics of System Under Blade Loss Events

In this section, dynamic characteristics of the system with blade loss are discussed under $n=5\,000$, 10 000 and 15 000 rev/min. It's worth noting that the broken blade will not be released from the disk until $t=5/f_r$ ($f_r=n/60$).

Vibration responses of disk mass center under $n=5\,000$ rev/min are shown in Fig. 4. Figs. 4(a, b) show that an instantaneous impact exists when $t=5/f_r$ because of sudden unbalance caused by blade loss. Fig. 4(c) depicts the motion trajectory of disk mass center before and after blade loss. Transient and steady vibration responses after blade loss are processed by Fourier transform (see Figs. 4(d, e)). The spectrums reveal that multiple frequencies such as $2f_r$, $3f_r$ and $3.7f_r$ accompanying with natural frequencies such as f_{n1} and f_{n3} occur. This can be attributed to rubbing nonlinearity between components. Fig. 4(f) gives the poincaré map of motion trajectory of disk mass center in the last $5/f_r$. Period-1 orbit can be observed clearly.

The time-history curve of rubbing force is shown in Fig. 5. Fig. 6 shows the contact states between components at local moments under $n=5\,000$ rev/min. Figs. 5(b—d) are the enlarged views of rubbing region A (see Fig. 5(a)). Broken blade firstly contacts with the casing (see Fig. 5(b) and Fig. 6(b)), then contacts with both blade components and casing (see Fig. 5(c) and Fig. 6(c)), and finally contacts with the casing again (see Fig. 5(d), Figs. 6(d, e)). Furthermore, contact status at other local moments is also added into Fig. 6. It's worth noting that no component is damaged and local plastic deformation exists under $n=5\,000$ rev/min (Fig. 6(f)).

Rubbing dynamic characteristics of rotor-bladed disk-casing system under $n=10\,000$ rev/min are shown in Figs. 7—9. Compared with vibration responses under $n=5\,000$ rev/min, response amplitude after blade loss is much larger than that before blade loss (see Figs. 7(a—c)). Besides, spectrums in Figs. 7(d, e) show that both multiple and fractional frequencies occur. Moreover, unlike f_{n1} being excited under $n=$

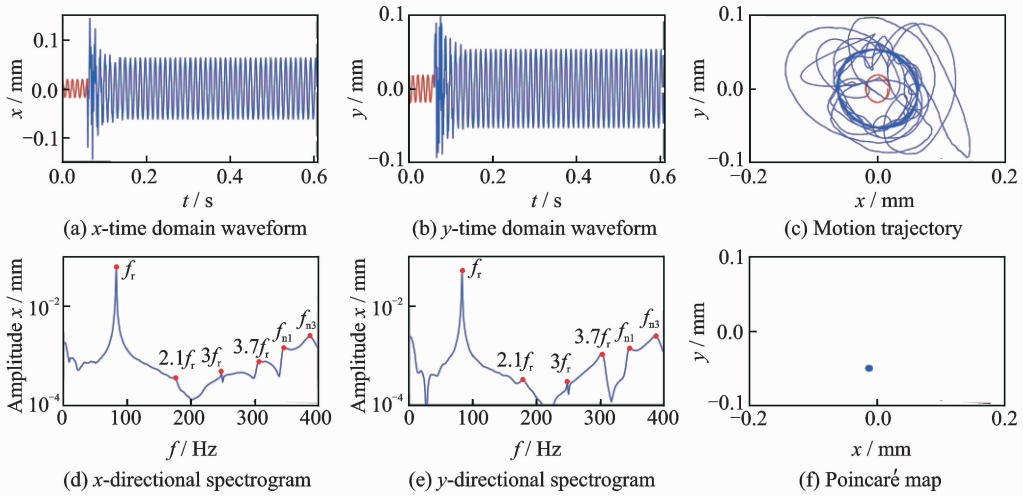

Fig. 4 Vibration responses of disk mass center and bearing dynamic anti-force under $n=5\ 000$ rev/min

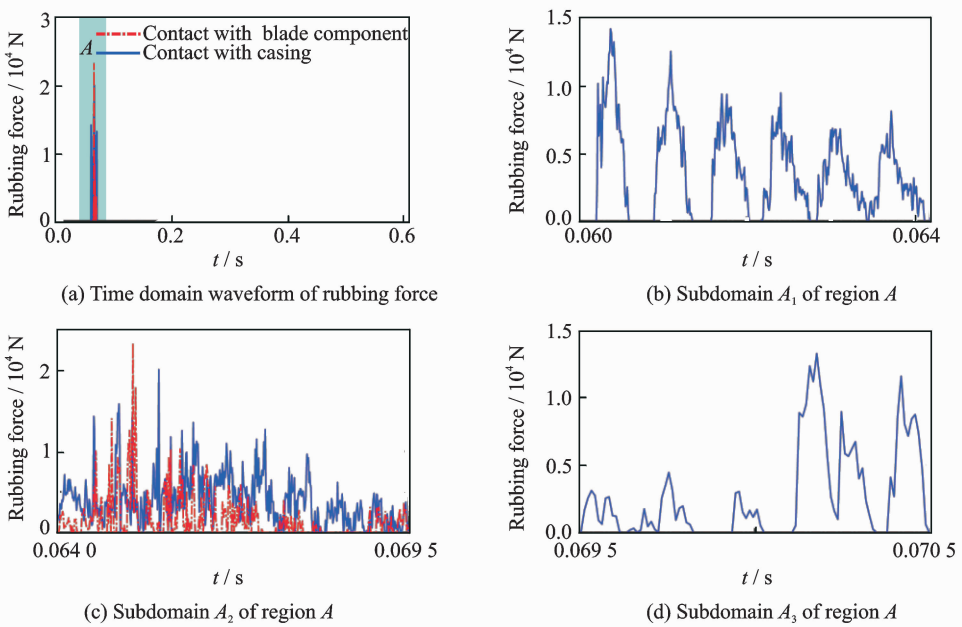

Fig. 5 Time-history curve of rubbing force under $n=5\ 000$ rev/min

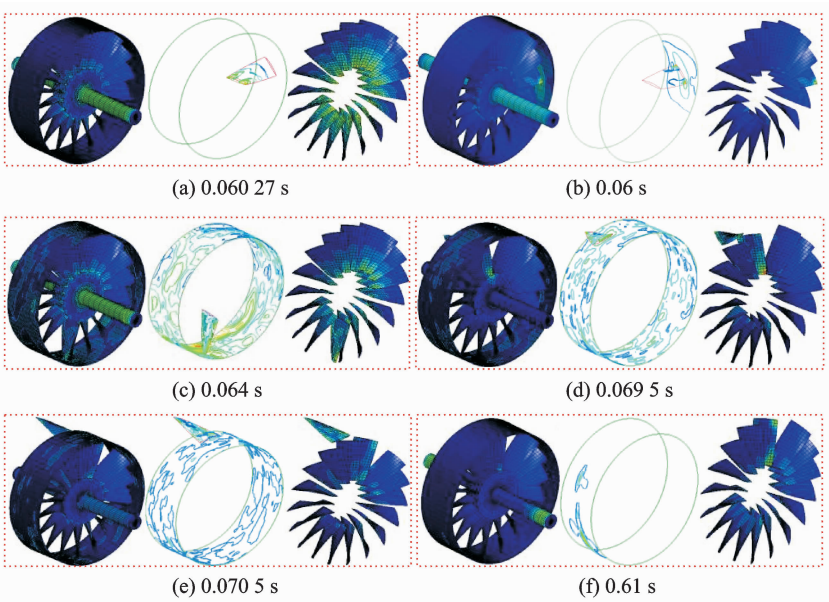

Fig. 6 Contact states between components at local moments under $n=5\ 000$ rev/min

5 000 rev/min (see Figs. 2 and 4), f_{n19} is excited here (see Figs. 2, 7). These phenomena indicate that rubbing becomes more severe. Poincaré map in Fig. 7(f) shows that the orbit of disk mass center also presents period-1 motion. Fig. 8 shows that both the contact time and amplitude of rubbing force are larger than those under n = 5 000 rev/min, which further validates the severity of rubbing. It's worth noting that the reason for period-1 motion of disk mass center is that there is no nonlinearity in the system during steady vibration process after blade loss (see Fig. 8, when $t \geqslant 0.098$ s, the rubbing force is 0 N). In Fig. 8(b), an interesting phenomenon is that blade component (see Fig. 1 (c)) also slightly contacts with casing when $t = 0.031\ 11$ s and 0.031 26 s. The reason causing this phenomenon is that when broken blade contacts with casing, local vibration of casing exists and the gap between blade component and casing then varies (see Figs. 9(a, b)), which leads to the occurrence of rubbing between casing and blade component.

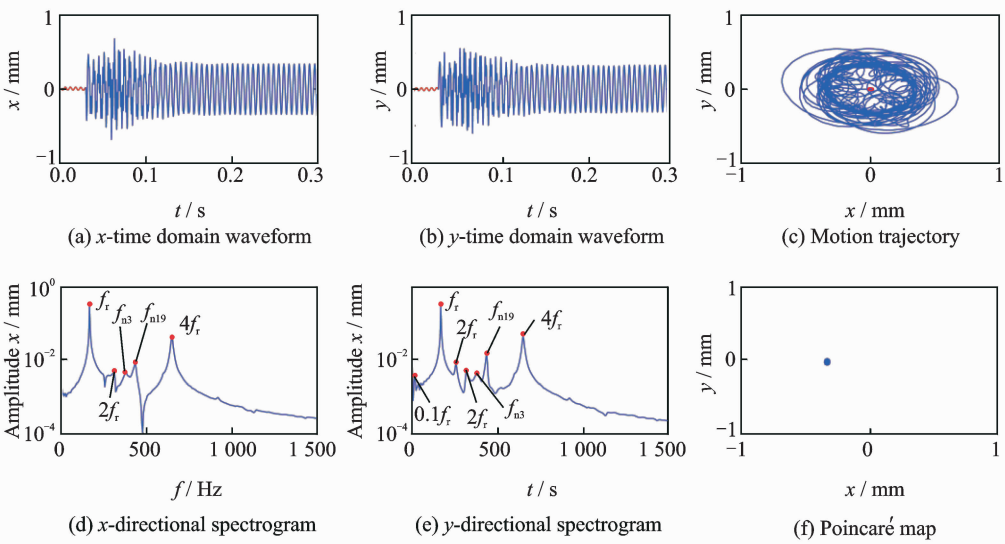

Fig. 7 Vibration responses of disk mass center and bearing dynamic anti-force under n=10 000 rev/min

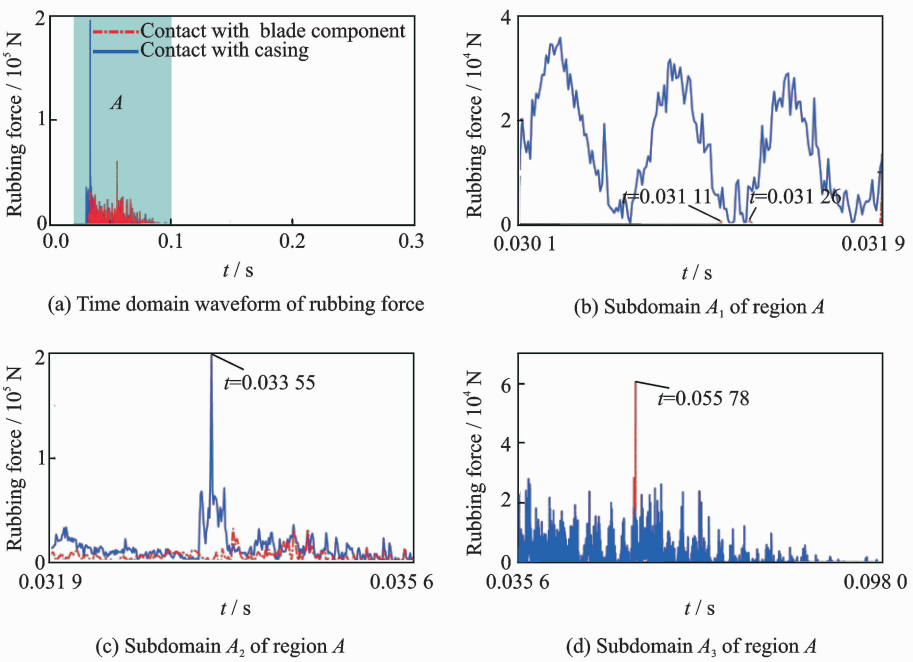

Fig. 8 Time-history curve of rubbing force under n=10 000 rev/min

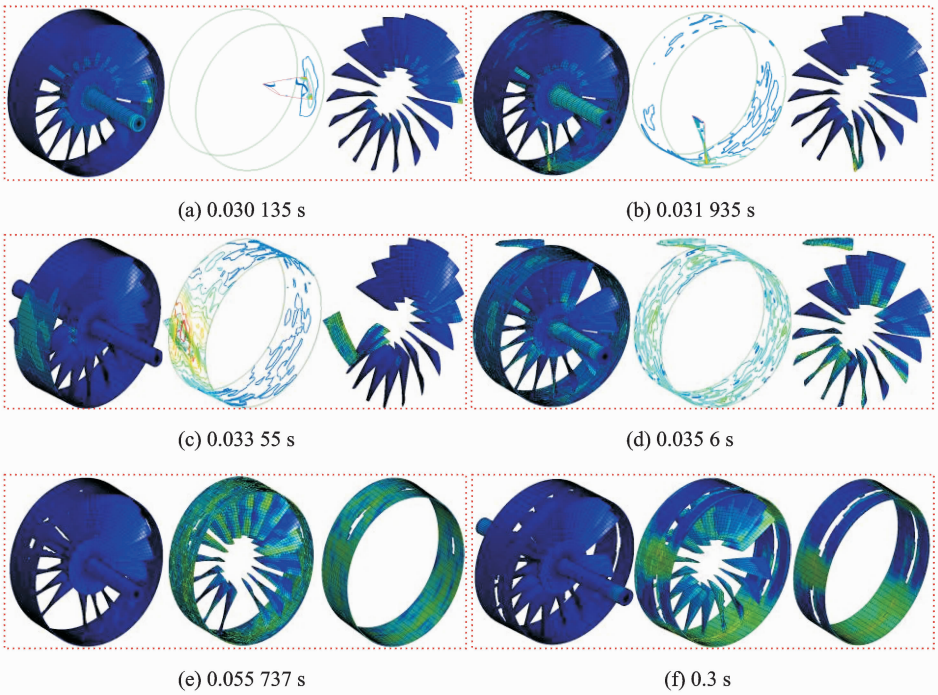

Fig. 9 Contact states between components at local moments under n=10 000 rev/min

When t= 0.033 55 s, there exists a peak in the curve representing the rubbing force of casing (see Fig. 8(c)). This phenomenon can be explained as follows: On the one hand, the broken blade makes centrifugal movement under the effect of centrifugal force and persistently impacts the casing, and the rubbing force can reach the maximum at certain moment, such as t = 0.033 55 s in this paper. On the other hand, assuming that the total energy is definited when rubbing between blade component and broken blade occurs, the rubbing force can be reduced because of large flexural deformation existing in the blade contacting with the broken blade (see Fig. 9(c)). Fig. 8(d) demonstrates that the rubbing force obtained from both blade component and casing are nearly the same except at the moment t=0.055 78 s. This also indicates that rubbing occurs between blade component and casing (see Figs. 9(d, e)). As for the occurrence of catastrophe point at t=0.055 78 s, it is because blade component contact with not only casing but also itself. In addition, Figs. 9(a, f) represent the initial and final contact states between components.

Figs. 10—12 show the rubbing dynamic behaviors of rotor-bladed disk-casing system under n=15 000 rev/min. Compared with vibration responses under n= 5 000, 10 000 rev/min, the distinct difference is the frequency component in the spectrum (see Fig. 10). Only natural frequency f_{n19} can be observed. Moreover, there also exist some differences in the time-history curve of rubbing force relative to the previous two cases (see Fig. 11). Rubbing force in Fig. 11(b) doesn't show multiple-pulse variation relative to that in Fig. 5(b) and Fig. 8(b). In Fig. 11(d), the rubbing force obtained from blade component always exists even if blade component has no contact with casing. This is mainly because permanent plastic deformation exists in the blade component leading to the appearance of self-contact in the blade. Fig. 12 gives the contact states of the system components at local moments. Fig. 12(a) represents that broken blade just contacts with casing. Fig. 12(b) shows the contact between broken blade, blade component and casing. In Fig. 12(c), casing is cut off by broken blade. Fig. 12(d) shows the final contact states when termination time is arrived.

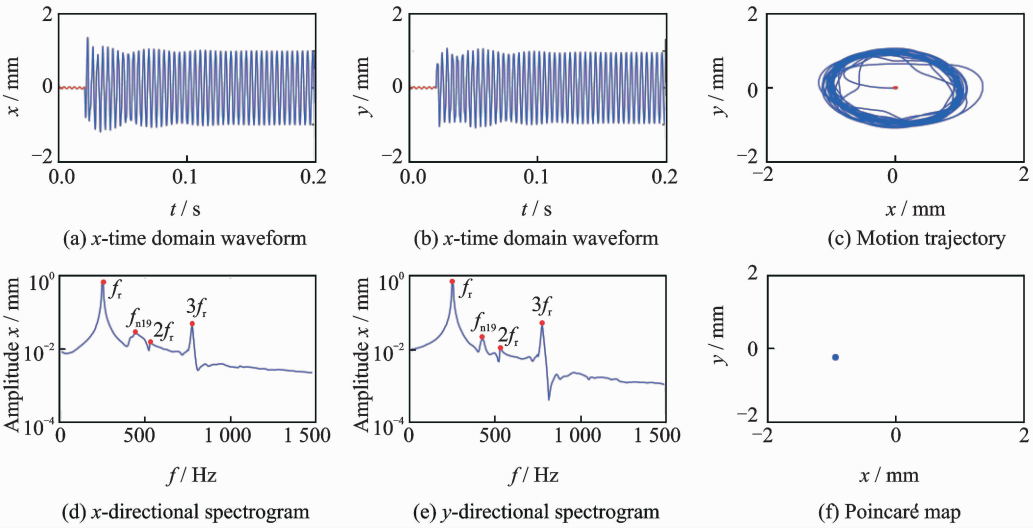

Fig. 10 Vibration responses of disk mass center and bearing dynamic anti-force under $n=15\ 000$ rev/min

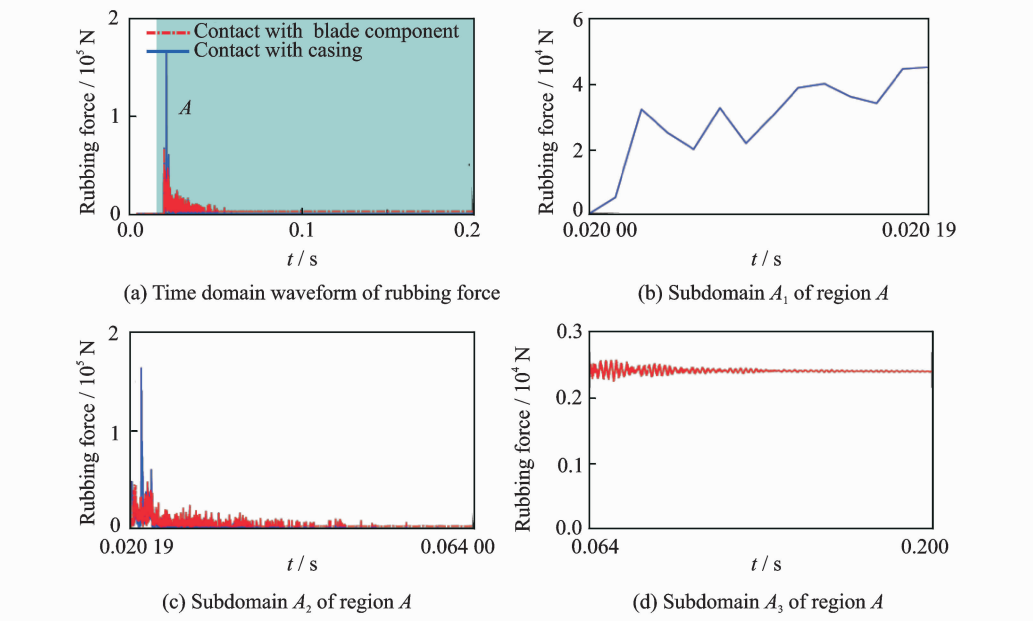

Fig. 11 Time-history curve of rubbing force under $n=15\ 000$ rev/min

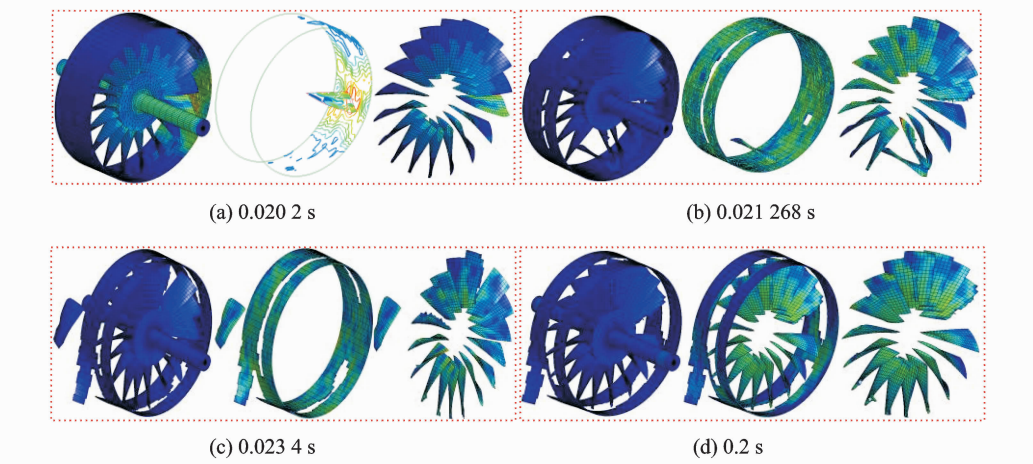

Fig. 12 Contact states between components at local moments under $n=15\ 000$ rev/min

3 Conclusions

The finite element model of rotor-bladed disk-casing is established using ANSYS/LS-DYNA. Then the effects of blade loss under different operational speeds on the rubbing dynamic characteristics of the system are analyzed in detail. Some conclusions can be made as follows:

(1) Contact between broken blade, blade component and casing is considerably nonlinear. Multiple frequencies even fractional frequency can exist in the rubbing responses caused by blade loss. Under low operational speed, free vibration in the rubbing responses mainly gives priority to one nodal diameter vibration of bladed disk coupling with the lateral vibration of the shaft as well as the first order bending vibration of blade. With the increasing operational speed, the first order bending vibration of blade in the rubbing responses gradually becomes indistinct, but the first order bending vibration of blade coupling with the lateral vibration of the shaft and disk becomes dominant.

(2) During rubbing process, three distinct rubbing phases can be observed under the given operational speeds in this paper. The first phase is the contact between broken blade and casing, the second phase is the mixed contact between broken blade, blade component and casing, and the rubbing mechanical behaviors in the third phase depend on the operational speed, i. e. , contact occurs between broken blade and casing under low operational speed but between blade component and casing under high operational speed. Moreover, self-contact in the blade may appear especially at high operational speed.

Acknowledgements

This work was supported by the National Natural Science Foundation of China (No. 11772089), the Fundamental Research Funds for the Central Universities (Nos. N160312001 and N160313004), and the Research Project of State Key Laboratory of Mechanical System and Vibration (No. MSV201707).

References:

[1] SILVA V R, KHATIB W, FLEMING P J. Performance optimization of gas turbine engine[J]. Engineering Applications of Artificial Intelligence, 2005,18(5):575-583.

[2] TAVIK G C, LI H, ZHANG X, XU F. Experimental investigation on centrifugal compressor blade crack classification using the squared envelope spectrum[J]. Sensors, 2013,13(9):12548-12563.

[3] CHIU Y J, CHEN D Z. The coupled vibration in a rotating multi-disk rotor system[J]. International Journal of Mechanical Sciences, 2011,53(1):1-10.

[4] WANG C, ZHANG D Y, MA Y H, et al. Dynamic behavior of aero-engine rotor with fusing design suffering blade off[J]. Chinese Journal of Aeronautics, 2017,30(3):918-931.

[5] MEHER-HOMJI C B, GABRILES G. Gas turbine blade failures—Causes, avoidance, and troubleshooting[C]//27th Turbomachinery Symposium. Houston, TX: [s. n.], 1998:20-24.

[6] LIU C, JIANG D. Crack modeling of rotating blades with cracked hexahedral finite element method[J]. Mechanical Systems and Signal Processing, 2014,46(2):406-423.

[7] WITEK L. Crack propagation analysis of mechanically damaged compressor blades subjected to high cycle fatigue[J]. Engineering Failure Analysis, 2011,18(4):1223-1232.

[8] JUNG C, SAITO A, EPUREANU B I. Detection of cracks in mistuned bladed disks using reduced-order models and vibration data[J]. Journal of Vibration and Acoustics, 2012,134(6):061010.

[9] SHMOTIN Y N, GABOV D V, RYABOV A A, et al. Numerical analysis of aircraft engine fan blade-out [J]. AIAA/ASME/SAE/ASEE Joint Propulsion Conference & Exhibit. [S. l.]:AIAA,2013.

[10] COSME N, CHEVROLET D, BONINI J, et al. Prediction of transient engine loads and damage due to hollow fan blade-off[J]. Revue Européenne des Eléments, 2002, 11(5): 651-666.

[11] GÁLVEZ F, CENDÓN D A, ENFEDAQUE A, et al. Materials behaviour and numerical simulation of a turbine blade-off containment analysis[J]. WIT Transactions on the Built Environment, 2006, 87: 12.

[12] CARNEY K S, LAWRENCE C, CARNEY D V.

Aircraft engine blade-out dynamics[C]//Seventh International LS-DYNA Users Conference. Livermore CA, USA: Livermore Software Technology Corporation, 2002:14-17.

[13] SUN G, PALAZZOLO A, PROVENZA A, et al. Long duration blade loss simulations including thermal growths for dual-rotor gas turbine engine[J]. Journal of Sound and Vibration, 2008, 316(1): 147-163.

[14] SINHA S K. Rotordynamic analysis of asymmetric turbofan rotor due to fan blade-loss event with contact-impact rub loads[J]. Journal of Sound and Vibration, 2013, 332(9): 2253-2283.

[15] JAIN R. Prediction of transient loads and perforation of engine casing during blade-off event of fan rotor assembly[J]. Scientist, 2010, 91: 9945082491.

[16] HEIDARI M, CARLSON D L, SINHA S, et al. An efficient multi-disciplinary simulation of engine fan-blade out event using MD Nastran [C]//49th AIAA/ASME/ASCE/AHS/ASC Structures, Structural Dynamics, and Materials Conference. Schaumburg, IL: AIAA, 2008: AIAA 2008-2333.

[17] HE Q, XUAN H, LIAO L, et al. Simulation methodology development for rotating blade containment analysis[J]. Journal of Zhejiang University—Science A, 2012, 13(4): 239-259.

[18] HE Q, XUAN H, LIU L, et al. Perforation of aero-engine fan casing by a single rotating blade[J]. Aerospace Science and Technology, 2013, 25(1): 234-241.

[19] HE Q, XIE Z, XUAN H, et al. Multi-blade effects on aero-engine blade containment[J]. Aerospace Science and Technology, 2016, 49: 101-111.

Mr. **Zeng Jin** received B. S. and M. A. degrees in School of Mechanical Engineering and Automation, Northeastern University in 2013 and 2016, respectively. In September 2016, he became a doctoral student at Northeastern University. His research is focused on rotor dynamics.

Prof. **Ma Hui** received B. S. degree in Liaoning Technical University in 2002 and Ph. D. degree in Northeastern University in 2007, respectively. From 2007 to present, he has been in the School of Mechanical Engineering and Automation, Northeastern University. In 2013 he was awarded the New Century Excellent Researcher Award Program from Ministry of Education of China. From Nov. 2014 to Oct. 2015, he worked as a visiting scholar in the University of Sheffield, England. His research interests include rotor dynamics and fault diagnosis.

Mr. **Ma Xinxing** received his B. S. degree from School of Mechanical and Electrical Engineering, Qingdao University in 2016. In September 2016, he became a post-graduate student at the School of Mechanical Engineering and Automation, Northeastern University. His research is focused on rotor dynamics.

Mr. **Wu Zhiyuan** received B. S. and M. A. degrees in School of Mechanical Engineering and Automation, Northeastern University in 2013 and 2015, respectively. Now he is a structural engineer in Shanghai Institute of Space Power-Sources.

Dr. **Qin Zhaoye** received B. S. degree in Northeastern University in 2006 and Ph. D. degree in Tsinghua University in 2010, respectively. From October 2010 to April 2013, he worked as a postdoctor in the Department of Precision Instruments and Mechanics, Tsinghua University. From 2013 to present, he has been in State Key Laboratory of Tribology, Department of Mechanical Engineering, Tsinghua University. In addition, he is an member of Chinese Society for Vibration Engineering. His research interests include rotor dynamics and vibration control.

(Production Editor: Sun Jing)